panded nozzles at low pressure ratios," Bull. Res. Council Israel **11C**, 45–55 (1962).

[6] Fortini, A. and Ehlers, R. C., "Comparison of experimental to predicted heat transfer in a bell-shaped nozzle with upstream flow disturbances," NASA TN D-1743 (August 1963).

[7] Stantion, T. E., "The variation of velocity in the neighborhood of the throat of a constriction in a wind channel," British Aeronautical Research Council R & M 1388 (1930).

[8] Elliott, D. G., Bartz, D. R., and Silver, S., "Calculation of turbulent boundary-layer growth and heat transfer in axi-symmetric nozzles," Jet Propulsion Lab. TR 32-387, Pasadena, Calif. (February 15, 1963).

[9] Hall, I. M., "Transonic flow in two-dimensional and axially-symmetric nozzles," Quart. J. Mech. Appl. Math. **XV**, 487–508 (1962).

[10] Sauer, R., "General characteristics of the flow through nozzles at near critical speeds," NACA TM-1147 (June 1947).

[11] Darwell, H. M. and Badham, H., "Shock formation in conical nozzles," AIAA J. **1**, 1932–1934 (1963).

[12] Migdal, D. and Landis, F., "Characteristics of conical supersonic nozzles," ARS J. **32**, 1898–1901 (1962).

[13] Oswatitsch, K. and Rothstein, W., "Flow pattern in a converging-diverging nozzle," NACA TM-1215 (March 1949).

[14] Jaivin, G. I., "Effect of hole size on pressure measurements made with a flat-plate dynamic-head probe," Jet Propulsion Lab. TR 32-617, Pasadena, Calif. (June 15, 1964).

[15] Livesey, J. L., Jackson, J. D., and Southern, C. J., "The static hole error problem," Aircraft Eng. **XXXIV**, 43–47 (1962).

[16] Ahlberg, J. H., Hamilton, S., Migdal, D., and Nilson, E. N., "Truncated perfect nozzles in optimum nozzle design," ARS J. **31**, 614–620 (1961).

[17] Arens, M. and Spiegler, E., "Shock-induced boundary layer separation in overexpanded conical exhaust nozzles," AIAA J. **1**, 578–581 (1963).

[18] Kolozsi, J. J., "An investigation of heat transfer through the turbulent boundary layer in an axially symmetric, convergent-divergent nozzle," Aerodynamic Lab., Ohio State Univ. TM-8 (July 1958).

SEPTEMBER 1965 AIAA JOURNAL VOL. 3, NO. 9

Viscous, Radiating Shock Layer about a Blunt Body

H. HOSHIZAKI* AND K. H. WILSON†
Lockheed Missiles & Space Co., Palo Alto, Calif.

The effect of radiation cooling on the radiative and convective heat-transfer distribution around a blunt body is investigated. An integral method is employed to obtain solutions to the appropriate equations. The gas in the shock layer is assumed to be viscous, radiating but nonabsorbing. Solutions to the direct, viscous blunt-body problem are obtained by means of an iterative procedure. The results for a 30° hemisphere-cone show that the loss of energy in the shock layer by radiation reduces both the radiative and convective heat transfer. This reduction was found to persist around the body. It was also found that the entropy layer increased the radiative heating on the conical afterbody by two orders of magnitude.

Nomenclature

a_i = velocity profile coefficients
b_i = enthalpy profile coefficients
C_i = mass fraction of species
C_p = total specific heat at constant pressure
$\bar{C}_p$ = frozen specific heat at constant pressure
D_{ij} = diffusion coefficient for a multicomponent system
$\mathfrak{D}_{ij}$ = diffusion coefficient for a binary system
E' = radiant emission per unit time per unit volume, $4\rho\lambda\sigma T^4$
F_i = boundary-condition functions defined in Sec. 3.3
f = velocity function, u/u_δ
g = enthalpy function, H/H_δ
h = static enthalpy
h_i = static enthalpy of ith species, including enthalpy of formation
H = total enthalpy
I_1 = momentum integral
I_2 = energy integral
k = total thermal conductivity
$\bar{k}$ = frozen thermal conductivity
m = exponent in Eq. (22a)
M_i = molecular weight of species i
n_i = moles of species i per unit volume
n_t = total number of moles per unit volume
P = static pressure
Pr = total Prandtl number, $Pr = C_p\mu/k$
$\dot{q}_c$ = convective energy flux
$\dot{q}_r$ = radiative energy flux
r = body radius measured from body centerline
R = body radius
$\tilde{R}e$ = Reynolds number, $\rho_\infty U_\infty R/\mu_\delta$
Re = Reynolds number, $\rho_{\delta,0} U_\infty R/\mu_{\delta,0}$
S = distance along shock wave
T = temperature
$\tilde{T}_1$ = reference temperature, 7200°K
u = velocity component parallel to body
U_∞ = freestream velocity
$\tilde{U}$ = velocity in 10^4 fps
v = velocity component normal to surface
$\bar{v}$ = velocity component normal to surface in shock-oriented coordinate system
X_i = mole fraction of species i, $X_i = n_i/n_t$
x, y = body-oriented coordinate system
β = velocity gradient
γ = isentropic index
δ = shock-detachment distance
$\tilde{\delta}$ = transformed shock-detachment distance, Eq. (5d)
δ_v = boundary-layer thickness
ϵ = difference between body and shock angle, also emissivity
η = Dorodnitzyn variable, Eq. (8a)
θ = body angle
κ = body curvature
$\tilde{\kappa}$ = $1 + \kappa y$
λ = mass absorption coefficient
$\tilde{\lambda}_1$ = reference mass absorption coefficient, 96.8 ft²/slug
μ = dynamic viscosity
ν = kinematic viscosity
ρ = density
$\tilde{\rho}$ = density ratio across shock, ρ_∞/ρ_δ
σ = Stefan-Boltzmann constant
ϕ = shock angle
ω = vorticity

Presented at the AIAA Entry Technology Conference, Williamsburg and Hampton, Va., October 12–14, 1964 (no preprint number; published in bound volume of preprints of the meeting); revision received May 5, 1965.

* Staff Scientist, Aerospace Sciences Laboratory. Member AIAA.

† Research Scientist, Aerospace Sciences Laboratory. Member AIAA.

Subscripts

ad = adiabatic (zero radiation loss)
0 = stagnation point
i = ith chemical species
w = wall quantities
δ = quantities immediately behind shock
∞ = freestream condition
( )′ = dimensional quantities and also differentiation

1. Introduction

THE aerodynamic heating that a space vehicle experiences when entering the earth's atmosphere at sub-satellite speeds is due primarily to convective heat transfer. The thermal radiation from the shock-heated gas in the shock layer contributes a negligible amount to the total heat transfer. At entry speeds approaching earth's escape velocity (approximately 37,000 fps), radiative heat transfer from the shock-layer gas to the vehicle surface is a significant fraction of the convective heat transfer. The precise ratio of radiative to convective heat transfer is a function of vehicle configuration, position along the body, flight velocity, and altitude. For most situations of interest at flight velocities near earth's escape velocity, the radiative heat transfer can be calculated by assuming the inviscid region of the shock layer, which is the primary source of radiant energy, to be essentially adiabatic. The decrease in the total energy of the shock-layer gas caused by energy being radiated away is generally insignificant. Only at entry speeds near twice satellite speeds and only for large bodies does the decrease in the total energy of the shock-layer gas become significant. This decrease in the shock-layer gas total energy by radiation is often referred to as the "radiation-cooling effect." The radiation-cooling effect can significantly alter the velocity, enthalpy, and density profiles in the shock layer. The convective and radiative heat transfer are also affected in that they are both reduced by significant amounts.

By means of a streamtube analysis, Bird[1] found that the velocity and pressure field in the shock layer of a blunt body are relatively insensitive to the loss of total enthalpy by radiation. His results suggested that the radiation processes in the shock layer can be uncoupled from the flow-field analysis. This is certainly the case when the radiation losses are small. When radiation losses are large the increase in shock-layer density will cause the shock wave to move in closer to the body.[2] The velocity field will thus be affected, but the pressure immediately behind the shock will not since the shock angle is only slightly altered. The surface pressure may or may not be affected depending on how dependent it is on the velocity and density profiles. Kennet[3] made use of Bird's conclusion that the velocity and pressure field are unaltered when the radiation loss is small, and calculated the enthalpy loss in the shock layer around a sphere using Lighthill's[4] inviscid, adiabatic solution. Both Bird and Kennet assumed the shock-layer gas to be transparent.

Goulard[5] has also analyzed radiative transfer in shock layers, using a simplified one-dimensional flow model. Both emission and absorption are taken into account. Approximate expressions were obtained for the temperature distribution and the radiative heat transfer at the stagnation point. Howe and Viegas[6] employed the local similarity assumption in analyzing the stagnation-point flow on a blunt body. Numerical solutions to the appropriate equations were obtained including the effects of emission and absorption, viscosity, and surface mass injection. The entire shock layer was assumed to be viscous to account for the inherent coupling between the inviscid and viscous flows. This coupling, which should not be confused with the coupling between the radiation loss and the inviscid flow field, is discussed in greater detail in Sec. 2.

Finally, Wilson and Hoshizaki[2] have considered the inviscid, nonadiabatic flow around a blunt body. An integral method was employed to determine the radiation-coupled flow field around a hemisphere. Coupling between the radiation loss and the flow field was taken into account for an optically thin shock layer in thermodynamic equilibrium.

The purpose of the present paper is to determine the convective and radiative heat transfer around a blunt body for conditions where the flow field is significantly affected by radiation loss. The coupling between radiation loss and the flow field and the inherent coupling between the inviscid and viscous regions of the shock layer are accounted for by assuming the shock-layer gas to be a viscous and radiating medium. The shock-layer gas is also assumed to be optically thin and in thermodynamic equilibrium. The effects of mass injection, self-absorption, and finite-rate chemistry are not considered in the present analysis. These additional effects are reserved for future consideration.

The thin shock approximations are used to simplify the complete equations of motion. An iterative integral method is used to determine the shock shape for a specified body shape. Because of the iterative integral method employed, the solution must be considered approximate in contrast to exact numerical solutions to the governing equations. The solutions obtained, however, are adequate for determining such gross quantities as convective and radiative heat transfer.

2. Discussion of the Problem

2.1 Coupling between Radiation-Loss, the Inviscid, and the Viscous Flow Regions

Whenever radiative transfer is included in an analysis of the flow around a blunt body, several interesting coupling effects arise. We can identify the following coupling effects: 1) the coupling between the loss of energy by radiation and the velocity, temperature, and density profiles in the inviscid region of the shock layer; 2) the inherent coupling between the inviscid and viscous region due to energy loss along those streamlines in the inviscid flow which subsequently enter the viscous flow region; and 3) the coupling in a transparent radiating gas between radiative and conductive energy transport caused by large temperature gradients in the inviscid flow near the wall.

The first coupling effect is created by the decrease in the total enthalpy of a fluid particle by radiation loss as it travels around the body. The cooling of the flow by radiation loss increases the density of the shock-layer gas causing the bow shock wave to move in closer to the body. This change in the shock-wave position is illustrated schematically in Fig. 1. Although the shock-detachment distance can be altered

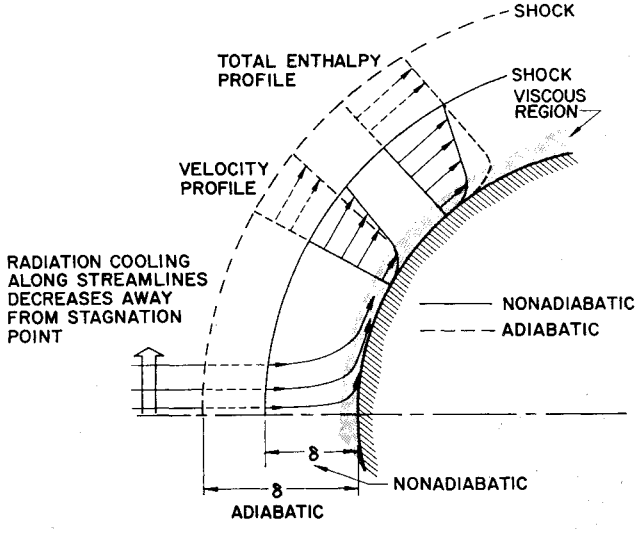

Fig. 1 Flow field schematic.

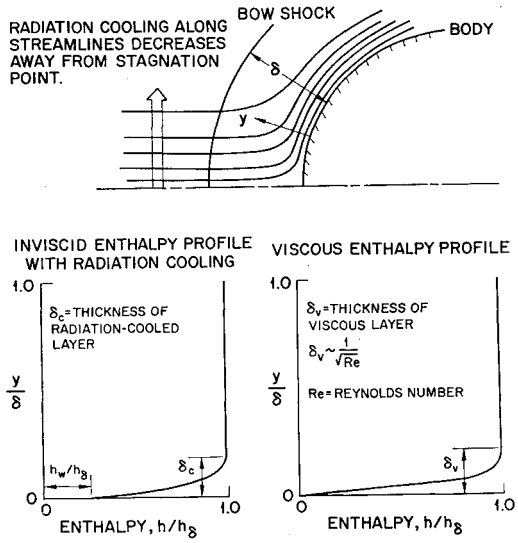

Fig. 2 Shock-layer enthalpy profiles.

significantly, the shock shape (angle) is much less sensitive to radiation cooling. Hence, the pressure field will be little affected whereas the density and velocity will be increased and the temperature decreased by radiation cooling. Although this coupling is most prominent in the inviscid-flow region, it is still present in the viscous region. The viscous region, however, is dominated by molecular transport processes.

The second coupling effect is due to the fact that a fluid particle can lose energy by radiation as it traverses the inviscid region of the shock layer prior to entering the viscous region. Since the radiation loss along streamlines decreases away from the stagnation point (Fig. 1), the total enthalpy of a fluid particle entering the viscous region will vary along the body. The total enthalpy at the edge of the viscous region will be a minimum at the stagnation point. This variation of the edge total enthalpy requires that the analysis of the viscous region be of a nonsimilar nature. The fluid particles entering the viscous region have a "past history," and in this sense the inviscid and viscous flow fields are coupled.

One can attempt to uncouple the inviscid flow-field analysis from the viscous analysis by first obtaining an inviscid, nonadiabatic solution to the shock-layer flow. The extent of the viscous region can then be estimated and the inviscid solution evaluated at the edge of the viscous region used as boundary conditions. In order to use a first-order boundary-layer analysis, the location of the viscous region edge must be picked such that the gradients in the inviscid flows are small. In an optically thin, radiating gas, large gradients are present in the inviscid flow near the wall. In fact, Goulard[5] obtains an infinite temperature gradient at the wall for the stagnation-point flow of a transparent gas. This leads us to the third coupling effect that is peculiar to a transparent, or near-transparent gas.

For an optically thin gas, boundary conditions for the viscous flow cannot be obtained by evaluating the inviscid solution at the wall since the total enthalpy vanishes, as was pointed out by Kennet[3] and discussed by Goulard.[5] Thomas[7] has shown that, for an absorbing gas, the wall enthalpy does not vanish but attains a value less than the value behind the shock.

The vanishing of the total enthalpy at the wall in the inviscid flow of a radiating, transparent gas can be explained by considering the flow along the stagnation streamline and those adjacent to it. Near the wall the velocity normal to the body along the stagnation streamline is proportional to its distance from the wall $v = -dy/dt \sim y$ so that $t \sim -\ln y$, and the time for a fluid particle to travel from the shock to the body surface along the stagnation streamline is infinite. If the gas only emits and does not absorb radiative energy, a fluid particle will radiate all of its energy away. Since the body surface streamline is a continuation of the stagnation streamline, the total enthalpy at the surface is also zero. Hence, the enthalpy driving potential for the convective heating vanishes.

On those streamlines adjacent to the stagnation streamline, the transit time is finite but large, and a fluid particle will lose a significant fraction of its total energy. The magnitude of the energy loss by radiation cooling decreases away from the stagnation point. This creates a radiation-cooled layer near the body surface as illustrated in Fig. 2. This radiation-cooled layer in the inviscid flow is characterized by large gradients. The existence of large gradients in the radiation-cooled layer indicates that molecular transport processes are important, and the inviscid flow is now coupled to the viscous flow.

Under the approximation of negligible self-absorption, the radiation-cooled layer will always be present regardless of the magnitude of the radiation loss. As the radiation loss decreases, the thickness of the radiation-cooled layer will decrease. The viscous layer thickness, on the other hand, is determined primarily by the Reynolds number. Whether or not the gradients near the wall are caused by radiation cooling or viscosity depends on the magnitude of the radiation loss and Reynolds number. In any event, molecular transport processes are important in the radiation-cooled layer and in the viscous layer.

In the present analysis, the shock-layer gas is assumed to be optically thin so that the third coupling effect is present. All of the preceding coupling effects can be accounted for by assuming the entire shock layer to be a viscous, radiating medium. This is the approach adopted in this paper.

It is recognized that the optically thin gas approximation cannot be justified for all entry conditions of interest. An analysis that makes use of the optically thin gas approximation will give qualitative and, for some situations, quantitative results on the effect of radiation cooling on the convective and radiative heat-transfer rates. The extension of the analysis presented in this paper to include self-absorption of radiant energy is currently under consideration.

3. Analysis of Radiating, Viscous Shock Layer

3.1. General Method of Solution

The problem considered in the present paper is to determine, for a given body shape, the structure of the shock-layer flow field when the shock layer is both viscous and radiating. One possible method of attacking this problem is to employ the method of integral relations as exemplified by the work of Belotserkovskii[8] for the inviscid case. In this method the shock layer is divided into n strips in the streamwise direction. Certain groups of physical variables are assumed to vary as polynomials across the strips and the equations integrated across the strips. Boundary conditions are matched at the strip boundaries. In this manner, the governing equations are reduced to total differential equations that are solved numerically by forward integration.

Another method is to use the inner and outer expansion technique, as employed by Van Dyke,[9] to investigate second-order boundary-layer effects. An inner and outer expansion is used to describe the flow in the inviscid and viscous regions, respectively. The two expansions are matched in an overlap region of common validity.

A third method is the integral method employed by Maslen and Moeckel[10] to investigate the inviscid blunt-body problem. This approach is basically similar to the Karman-Pohlhausen[11] momentum integral method extensively used in boundary-layer analyses. In the present analysis this integral method is employed. The governing equations are first simplified

by assuming the shock layer to be thin, i.e., $\delta \ll 1$. In addition, the viscous region is assumed to extend out to the shock wave that defines the lower limit in Reynolds number. The shock wave itself is assumed to be a discontinuity. The simplified equations are then integrated across the shock layer to obtain integrodifferential equations in one independent variable. The integrals are evaluated by assuming that the velocity and enthalpy profiles in the shock layer can be represented by suitable polynomials.

The symmetry conditions at the stagnation point yield all but one necessary boundary condition to treat the problem as an initial value problem. The unknown boundary condition is either the stagnation-point shock-detachment distance or the shock curvature. In the present analysis, solutions are obtained by an iteration procedure. An initial guess is made for the shock angle as a function of body position. The equations are then solved to obtain a complete description of the shock-layer flow field. A new shock shape is computed which forms the basis of the second iteration. The procedure is repeated until satisfactory convergence is obtained.

3.2. Governing Equations

The governing equations are obtained by simplifying the complete conservation equations[12] for a multicomponent, continuum gas in thermodynamic equilibrium. Both the thin-shock approximations and boundary-layer-type approximations are used in an order-of-magnitude analysis to reduce the complete equations to a set of equations that are correct to $O(\rho)$.

For the purpose of evaluating the viscous terms, assume that the viscous region extends out to the shock wave so that $\delta \approx \delta_v$ where δ and δ_v are the shock-detachment distance and the thickness of the viscous region, respectively. Since $\delta \sim \bar{\rho}$ and $\delta_v \sim 1/(Re)^{1/2}$, $\bar{\rho} \sim 1/(Re)^{1/2}$. We now normalize the normal velocity and distance by

$$v = [v'(Re)^{1/2}]/U \qquad y = [y'(Re)^{1/2}]/R$$

The convective terms are simplified by neglecting all terms of $O(\bar{\rho}^2)$ and higher, whereas the viscous terms are simplified by neglecting terms of $O(1/Re)$ and higher. Hence, the analysis is valid when the shock layer is completely viscous and, within our ability to accurately represent the shock-layer velocity and enthalpy profiles, when the viscous region is confined to a thin layer within the shock layer. The lower limit in Reynolds number is imposed by our use of the usual Rankine-Hugoniot shock relations that neglect molecular-transport processes immediately behind the rock.

The governing equations valid to $O(\bar{\rho})$ are

x momentum

$$\left(\frac{r'}{r_w'}\right)^n \rho'\bar{\kappa}'\left[u'\frac{\partial u'}{\partial x'} + \bar{\kappa}'v'\frac{\partial u'}{\partial y'} + \kappa' u'v'\right] = -\frac{\partial P'}{\partial x'} + \frac{\partial}{\partial y'}\left[\left\{\left(\frac{r'}{r_w'}\right)^n + 2\kappa' y'\right\}\mu'\frac{\partial u'}{\partial y'} - \kappa'\mu' u'\right] \quad (1)$$

y momentum

$$\rho'\kappa' u'^2 = \partial P'/\partial y' \quad (2)$$

energy

$$\rho'\left(\frac{r'}{r_w'}\right)^n\left[u'\frac{\partial H'}{\partial x'} + \bar{\kappa}'v'\frac{\partial H'}{\partial y'}\right] = \frac{\partial}{\partial y'}\left[\frac{\mu'}{\bar{\kappa}'}\left\{\left(\frac{r'}{r_w'}\right)^n + 2\kappa' y'\right\}\left\{\frac{\partial H'}{\partial y'} + \left(\frac{1}{Pr} - 1\right)\frac{\partial h'}{\partial y'}\right\}\right] - \kappa'\frac{\partial}{\partial y'}(\mu' u'^2) - \bar{\kappa}'\left(\frac{r'}{r_w'}\right)^n E' \quad (3)$$

$$(\partial/\partial x')(r'^n\rho' u') + (\partial/\partial y')(r'^n\bar{\kappa}'\rho' v') = 0 \quad (4)$$

The body-oriented coordinate system used is shown in Fig. 3.

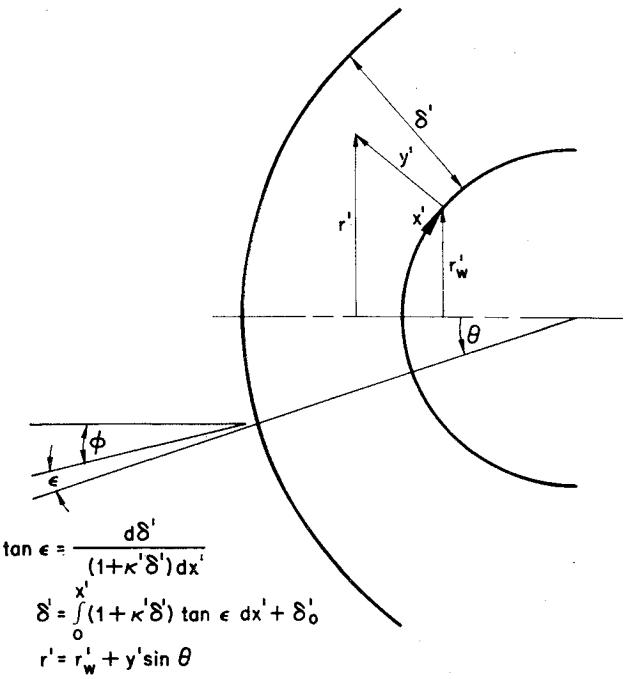

Fig. 3 Body-oriented coordinate system.

Mass diffusion of chemical species due to temperature and pressure gradients and external forces have been neglected. Mass diffusion due to concentration gradients, however, is accounted for by means of the total property concept.[13] For a transparent gas, the radiation-transfer term reduces to the simple form as given by the last term in the energy equation where E' is the radiant energy emission per unit volume per unit time. Note that the preceding equations are the boundary-layer equations with the addition of the curvature terms. The y momentum equation in the form used previously expresses the balance between centrifugal and pressure forces. It is used in this form to manipulate the streamwise-pressure-gradient term in the x momentum equation. For evaluating the pressure distribution across the shock layer, an approximate solution to the complete y momentum is employed.

The momentum and energy equations are integrated across the shock layer to reduce the governing equations to a set of total differential equations. A solution to these equations will satisfy the momentum and energy equation in the large. Only the tangential momentum and energy equations are actually integrated. The continuity equation is used to evaluate the normal velocity component, whereas the normal momentum equation is used to manipulate the pressure-gradient term into a form suitable for integration. The analysis at this point follows closely the work of Maslen and Moeckel[10] for the inviscid flow about a blunt body. The addition of the viscous and radiation terms presents no difficulty.

In the analysis to follow, the variables are nondimensionalized in the following manner:

$$u = \frac{u'}{U_\infty'} \qquad \xi = \frac{x'}{R'} \qquad \delta = \frac{\delta'}{R'}$$

$$v = \frac{v'}{U_\infty'} \qquad y = \frac{y'}{R'} \qquad \tilde{\delta} = \frac{\tilde{\delta}'}{R'}$$

$$E = \frac{E'R'}{\rho'(U_\infty')^3} \qquad \rho = \frac{\rho'}{\rho_{\delta,0}'} \qquad \mu = \frac{\mu'}{\mu_{\delta,0}'}$$

$$\kappa = \kappa' R' \qquad H = \frac{H'}{H_\delta'} \qquad P = \frac{P'}{\rho_\infty' U_\infty'^2}$$

$$\bar{\kappa} = 1 + \kappa y \qquad h = \frac{h'}{H_\delta'} \qquad r = \frac{r'}{R'}$$

The compressibility effects can be reduced significantly by introducing the Dorodnitzyn variable defined by

$$\eta = \int_0^y \left(\frac{r}{r_w}\right)^n \rho\, dy \Big/ \int_0^\delta \left(\frac{r}{r_w}\right)^n \rho\, dy \tag{5a}$$

so that

$$y = \tilde{\delta} \int_0^\eta \left(\frac{r_w}{r}\right)^n \frac{1}{\rho}\, d\eta \tag{5b}$$

and

$$\delta = \tilde{\delta} \int_0^1 \frac{1}{\rho}\, d\eta - n\tilde{\delta}^2 \frac{\sin\theta}{2r_w} \left(\int_0^1 \frac{1}{\rho}\, d\eta\right)^2 \tag{5c}$$

where

$$\tilde{\delta} = \int_0^\delta \left(\frac{r}{r_w}\right)^n \rho\, dy \tag{5d}$$

Integration of the momentum and energy equations across the shock layer and transformation into the ξ, η variables results in the following integrodifferential equations:

Momentum

$$\frac{dI_1}{d\xi} + \left[\frac{2}{u_\delta}\frac{du_\delta}{d\xi} + \frac{n}{r_w}\frac{dr_w}{d\xi}(1 + \delta\kappa)\right] I_1 - \left(1 + \frac{n\delta\sin\theta}{r_w}\right)\rho_\delta \frac{d\delta}{d\xi} - \frac{d\kappa}{d\xi}\tilde{\delta}^2 \int_0^1 \left(f^2 \int_0^\eta \frac{d\bar{\eta}}{\rho}\right) d\eta + \left[1 + \delta\left(\frac{n\sin\theta}{r_w} + 2\kappa\right)\right]\frac{v_\delta}{u_\delta} = -\frac{\delta\rho_0}{u_0^2}\left(\frac{\partial P}{\partial\xi}\right)_\delta + \frac{1}{\tilde{\delta}u_\delta Re}\left[\left\{1 + 2\delta\left(\frac{n\sin\theta}{r_w} + \kappa\right)\right\} \times (\rho\mu)_\delta f'(1) - \mu_\delta\tilde{\delta}\kappa - (\rho\mu)_w f'(0)\right] \tag{6}$$

Energy

$$\frac{dI_2}{d\xi} + \left(\frac{1}{u_\delta}\frac{du_\delta}{d\xi} + \frac{n}{r_w}\frac{dr_w}{d\xi}\right) I_2 + \left[1 + \delta\left(\frac{n\sin\theta}{r_w}\right) + \kappa\right] \times \frac{\rho_\delta v_\delta}{u_\delta} - \left(\frac{r_\delta}{r_w}\right)^n \rho_\delta \frac{d\delta}{d\xi} = \frac{1}{\tilde{\delta}u_\delta Re}\left[\left\{1 + \delta\left(\frac{2n\sin\theta}{r_w} + \kappa\right)\right\} \times \left\{g'(1) + \left(\frac{1}{Pr_\delta} - 1\right)[g'(1) - 2u_\delta^2 f'(1)]\right\} \times (\rho\mu)_\delta - \frac{(\rho\mu)_w}{Pr_w} g'(0)\right] - \frac{2\kappa u_\delta \mu_\delta}{Re} - \frac{2\tilde{\delta}}{u_\delta}\int_0^1 \bar{\kappa}E\, d\eta \tag{7}$$

where

$$I_1 = \tilde{\delta}\int_0^1 f^2\, d\eta \tag{8a}$$

$$I_2 = \tilde{\delta}\int_0^1 fg\, d\eta \tag{8b}$$

$$f = u/u_\delta \tag{8c}$$

$$g = H/H_\delta \tag{8d}$$

and primes on f and g denote differentiation. In addition, the following approximation was used to obtain the second term in the momentum equation:

$$\bar{\kappa}_\delta I_1 \approx \tilde{\delta}\int_0^1 \bar{\kappa} f^2\, dy$$

The y momentum [Eq. (2)], correct to $O(\bar{\rho})$ with respect to terms in the x momentum equation, is used in the integration of the x momentum across the shock layer. To determine the pressure variation across the shock layer, the y momentum equation, correct to $O(\bar{\rho})$ with respect to the normal pressure gradient, is employed. This equation is the inviscid y momentum equation. The pressure variation is necessary to determine the density and emission profiles in the shock layer. By assuming that $v = v_1 \cdot \eta$, integration of the y momentum yields

$$P = P_\delta + \frac{\tilde{\delta}u_\delta}{\bar{\rho}_0}\left(\frac{dv_\delta}{d\xi}\right)_\delta\left(\int_0^1 \eta f\, d\eta - \int_0^\eta \eta f\, d\eta\right) + \frac{v_\delta^2}{\bar{\rho}_0}\left(\int_0^1 \rho\eta\, d\eta - \int_0^\eta \rho\eta\, d\eta\right) - \frac{\tilde{\delta}\kappa u_\delta^2}{\bar{\rho}_0} \times \left(\int_0^1 f^2\, d\eta - \int_0^\eta f^2\, d\eta\right) \tag{9}$$

The integrated momentum and energy equations express conservation of momentum and energy in the large. In the present formulation of the integral method, these equations are considered to define the momentum integral I_1 and the energy integral I_2. The integrals, however, are functions of the velocity and enthalpy profiles. The profiles will be expressed in terms of the shock shape and one unknown parameter, the enthalpy gradient at the wall. In principle, one can evaluate the integrals I_1 and I_2 [Eqs. (8a) and (8b)] and, by substituting the results into the integrated momentum and energy equations [Eqs. (6) and (7)], reduce the unknown quantities to the shock shape and the wall enthalpy gradient. The method is then quite analogous to that used in boundary-layer theory. In the present analysis, the integrated momentum and energy equations are used to determine I_1 and I_2, and the definitions of I_1 and I_2 [Eqs. (8a) and (8b)] are used to determine a transformed shock-detachment distance and the wall enthalpy gradient.

3.3 Velocity and Enthlapy Profiles and Boundary Conditions

The velocity and enthalpy profiles are assumed to be representable by polynomials in η where the coefficients are functions of the streamwise variable ξ. The coefficients are determined from boundary conditions applied at the wall and immediately behind the shock. The shock boundary conditions are the usual Rankine-Hugoniot relations that can be expressed as follows:

$$u_\delta = \sin\phi\sin\epsilon + \bar{\rho}\cos\phi\sin\epsilon \tag{10a}$$

$$v_\delta = \sin\phi\sin\epsilon - \bar{\rho}\cos\phi\cos\epsilon \tag{10b}$$

$$P_\delta = (1 - \bar{\rho})\cos^2\phi \tag{10c}$$

and for later use note that (Fig. 3)

$$\epsilon = \theta - \phi = \tan^{-1}[(d\delta/d\xi)/(1 + \kappa\delta)] \tag{10d}$$

Fifth- and sixth-order polynomials are used to represent the velocity and total enthalpy profiles, respectively:

$$\frac{u}{u_\delta} = f = \sum_{i=0}^{5} a_i\eta^i \tag{11}$$

$$\frac{H}{H_\delta} = g = \sum_{i=0}^{6} b_i\eta^i \tag{12}$$

Twelve boundary conditions will be specified which will enable 12 of the 13 coefficients to be expressed in terms of the remaining coefficient and the shock shape. The energy integral I_2 is used to determine the remaining coefficient.

The six boundary conditions on the velocity profile are as follows:

1) $\eta = 0$, $u = 0$ or $f(0) = 0$

2) $\eta = 0$, $\partial P'/\partial x' = (\partial/\partial y')[\mu'(\partial u'/\partial y')]$; this boundary condition is the momentum equation evaluated at the wall, neglecting curvature terms, and upon transforming becomes

$$f''(0) = \left(\frac{\partial P}{\partial\xi}\right)_w \frac{\tilde{\delta}^2\bar{\rho}Re}{(\rho\mu)_w u_\delta}\cdot\frac{\rho_\delta}{\rho_w} = F_0 \tag{13}$$

3) $\eta = 1, u = u_\delta$ or $f(1) = 1$ (14)

4) $\eta = 1, v = v_\delta$; by means of the continuity equation, this boundary condition can be written as

$$\int_0^1 f\,d\eta = \frac{1}{n+1}\left(\frac{r_\delta}{r_w}\right)^{n+1}\frac{r_w\bar{\rho}}{\tilde{\delta}u_\delta} = F_1 \tag{15}$$

and is equivalent to an over-all mass balance.

5) $\eta = 1, \omega' = \omega_\delta'$; this boundary condition is equivalent to satisfying the inviscid tangential momentum equation behind the shock. For strong shock waves,

$$-\omega_\delta' = \left(\frac{\partial u'}{\partial y'} + \frac{u'\kappa'}{\bar{\kappa}'}\right) = \frac{1}{\bar{\rho}}(1-\bar{\rho})^2 U_\infty' \sin\phi\frac{d\phi}{ds'} = f'(1)\frac{u_\delta'\bar{\rho}_\delta}{\tilde{\delta}}\left(\frac{r_\delta}{r_w}\right)^n + \frac{u_\delta'\kappa'}{\bar{\kappa}_\delta'}$$

Solving for $f'(1)$ and after some manipulation

$$f'(1) = \frac{\rho_\delta\tilde{\delta}}{\left(1+\frac{n\delta\sin\theta}{r_w}\right)^n}\left[\frac{(1/\bar{\rho}-2)(d\phi/d\xi)}{\left(\frac{\cos\epsilon}{\cos\varphi}+\bar{\rho}\frac{\sin\epsilon}{\sin\varphi}\right)\left[\frac{dr_w}{d\xi}+(1+\kappa\delta)\tan\epsilon\sin\theta+\frac{\delta}{L}\cos\theta\frac{d\theta}{d\xi}\right]}-\kappa\right] = F_2 \tag{16}$$

6) $\eta = 1, \partial^2 u'/\partial y'^2 = 0$ or $f''(1) = 0$ (17)

The six boundary conditions used to evaluate the coefficients in the enthalpy profile are as follows:

1) $\eta = 0, H = H_w$ or $g(0) = g_w$ (18)

2) $\eta = 0, (\partial/\partial y')[\mu'\{\partial H'/\partial y' + (1/Pr - 1)\partial h'/\partial y'\}]_w = 0$. This is the energy equation evaluated at the wall, neglecting curvature terms. By assuming that, near the wall, $\rho\mu = \text{const}$, this boundary condition can be written as

$$g''(0) = 2(1-Pr_w)u_\delta^2[f'(0)]^2 = F_3 \tag{19}$$

3) $\eta = 1, H = H_\delta$ or $g(1) = 1$ (20)

4) $\eta = 1, \partial H'/\partial y' = -E'/(\cos\epsilon\,\rho'\bar{v}_\delta'), \bar{v}_\delta' = -\rho U_\infty'\cos\phi$ which is the energy equation evaluated behind the shock where $\partial H'/\partial s' = 0$. In the transformed coordinate system,

$$g'(1) = (2\tilde{\delta}E/\bar{v}_\delta\rho_\delta^2)(r_w/r_\delta)^n = F_4 \tag{21}$$

5) $\eta = 1, \partial^2 H'/\partial y'^2 = -(\partial/\partial y')(E'/\rho'v')$. This equation is the derivative of the energy equation obtained by assuming that the shock wave is concentric so that $\partial H'/\partial s' = \partial H'/\partial x' = 0$. It provides a boundary condition on the second derivative of the enthalpy profile:

$$g''(1) = (\cos\phi\cos\epsilon/\cos\theta)\,g'(1)[mg'(1) - 1] = F_5 \tag{22}$$

where m is the exponent in the relation

$$E' \propto H^m \tag{22a}$$

6) $\eta = 1, \partial^4 H'/\partial y'^4 = 0$ or $g''''(1) = 0$ (23)

By means of the preceding twelve boundary conditions, twelve coefficients in the velocity and enthalpy profiles can be expressed in terms of the F_i functions that are functions only of the shock shape and the transformed standoff distance $\tilde{\delta}$. The velocity profile coefficients are

$$\left.\begin{aligned} a_0 &= 0\\ a_1 &= F_2 + 10F_1 - \tfrac{1}{12}F_0 - 5\\ a_2 &= \tfrac{1}{2}F_0\\ a_3 &= -10F_2 - 60F_1 - F_0 + 40\\ a_4 &= 15F_2 + 80F_1 + \tfrac{5}{6}F_0 - 55\\ a_5 &= -6F_2 - 30F_1 - \tfrac{1}{4}F_0 + 21 \end{aligned}\right\} \tag{24}$$

whereas the total enthalpy profile coefficients are

$$\left.\begin{aligned} b_0 &= g_w\\ b_2 &= \tfrac{1}{2}F_3\\ b_3 &= F_5 - \tfrac{20}{3}F_4 - \tfrac{11}{6}F_3 - \tfrac{25}{3}b_1 - 15g_w + 15\\ b_4 &= -\tfrac{5}{2}F_5 + 15F_4 + \tfrac{5}{2}F_3 + 15b_1 + 30g_w - 30\\ b_5 &= 2F_5 - 11F_4 - \tfrac{3}{2}F_3 - 10b_1 - 21g_w + 21\\ b_6 &= -\tfrac{1}{2}F_5 + \tfrac{8}{3}F_4 + \tfrac{1}{3}F_3 + \tfrac{7}{3}b_1 + 5g_w - 5 \end{aligned}\right\} \tag{25}$$

The transformed shock-detachment distance and the remaining coefficient b_1 are obtained from the momentum and energy integrals I_1 and I_2:

$$\tilde{\delta} = I_1\Big/\int_0^1 f^2\,d\eta \tag{26}$$

$$b_1 = \{I_2/\tilde{\delta} - [\ldots]\}\{1/[\ ]\} \tag{27}$$

These equations along with the expressions for a_i, b_i, and F_i, plus the integrated momentum and energy equations [Eqs. (7) and (8)] and the transformation relation Eq. (5c), complete the formulation of the problem. We can solve the preceding set of equations provided that the thermodynamic, transport, and optical properties of the gas are known.

3.4 Thermodynamic, Transport, and Radiative Properties

The analysis up to this point is valid for any multicomponent gas in thermodynamic equilibrium that emits but does not absorb radiation. Numerical solutions can be obtained if the thermodynamic, transport, and radiative properties are known. In the present paper, numerical results are obtained only for air. The thermodynamic and transport properties as computed by Hansen[14] and correlated by Viegas and Howe[15] are used in the numerical solutions. The correlation formulas are valid for temperatures between 1000° and 15,000°K and for pressures between 0.1 and 100 atm.

An upper-bound and a lower-bound estimate for the emissivity of air[2] along with the results of Kivel and Bailey[16] are used to determine the emission of radiant energy. These three values for the emissivity of air are used because of the present uncertainty in the radiative properties of air.

4. Numerical Method

The first step in the numerical method of solution is to obtain a solution at the stagnation point. The integrated momentum and energy equations, Eqs. (6) and (7), are first multiplied by u_δ. Since $u_\delta = 0$ at the stagnation point, the derivatives $dI_1/d\xi$ and $dI_2/d\xi$ are eliminated, and the equations reduce to algebraic equations. These two equations along with the equations that define the F_i's, a_i's, b_i's, I_1, I_2, and δ can be solved provided the $d\phi/d\xi$ is known. With an initial guess for the shock curvature, the complete stagnation-point solution can be obtained.

The solution downstream of the stagnation point proceeds as follows. An initial guess is made for $d\epsilon/d\xi$ as a function ξ where ϵ is the difference between the body and shock angle. Single and double integration of $d\epsilon/d\xi$ yields the shock angle and the shock-detachment distance.

The constants of integration are determined from the stagnation-point solution. It can be shown from symmetry conditions that $dI_1/d\xi = dI_2/d\xi = 0$ at the stagnation point. The value of I_1 and I_2 at the next integration point is obtained by forward integration. With I_1 and I_2 known and the shock

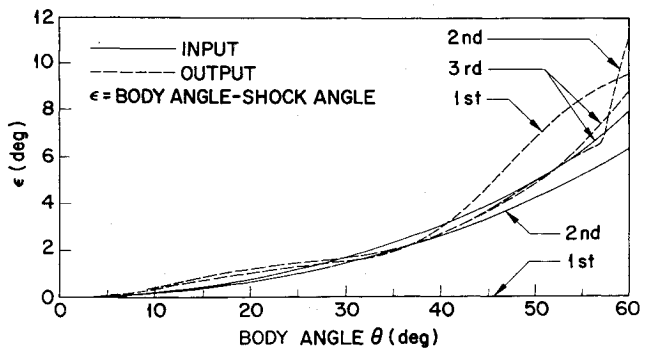

Fig. 4 Shock shape convergence.

shape completely specified, the F_i functions, the profile coefficients a_i and b_i, and $\tilde{\delta}$ can be calculated. Equation (5c) is then used to compute a new δ using the solution just obtained. The integrated momentum and energy equations are now used to evaluate $dI_1/d\xi$ and $dI_2/d\xi$. This completes a cycle and the procedure is repeated around the body. The shock angle is obtained from the computed shock-detachment distance and compared with the assumed values. The procedure is repeated until satisfactory convergence is obtained.

5. Discussion of Results

Numerical solutions were obtained for both hemispheres and hemisphere cones, with and without radiation-loss effects. In all the solutions, it was assumed that the density ratio across the shock was a constant, that is, $\rho_\delta = 1$. This assumption is justified at high flight velocities since the density ratio across the shock wave is practically independent of the flight velocity.[17] In addition, in the expression for the boundary condition on $g''(1)$, the exponent m, which relates the emission coefficient to the static enthalpy, was set equal to 5. This is a good approximation at high enthalpy levels when the boundary condition on $g''(1)$, which is the only quantity affected by the choice of m, becomes important. At low enthalpy levels, $g''(1) \approx 0$, independent of m.

The convergence of the iteration method used in the present numerical solution is demonstrated in Fig. 4. The quantity upon which convergence is based is ϵ, the difference between the body angle and the shock angle. The input for the $i + 1$ iteration is based on the results obtained for $d\epsilon/d\xi$ from the ith iteration. The input data were smoothed by inspection to expedite convergence.

Stagnation-point velocity and enthalpy profiles obtained by the present integral method are compared with the exact numerical solution of Howe and Viegas[6] in Fig. 5. The integral solution for the 250,000-ft-alt case presented in Fig. 5 does not include radiation-loss effects. The Howe and Viegas solution is essentially a zero radiation-loss case, and one can meaningfully compare the two results. The integral method is seen to reproduce the exact numerical results for the two flight conditions considered except for a small region in the shock layer.

The convective and radiative heat-transfer distributions on a hemisphere are presented in Fig. 6. Both the convective and radiative heat transfer are reduced by the radiation-cooling effect. This reduction in heat transfer is seen to persist around the hemisphere for both convection and radiation. The magnitude of the reduction is a function of the emissivity data used. The convective heat-transfer distribution without radiation loss is seen to fall below the boundary-layer similarity solution of Cohen.[18] The boundary-layer solution is based on the pressure distribution obtained by the present integral method. Similar discrepancies between nonsimilar integral solutions and self-similar boundary-layer solutions were noted previously by Libby.[19] One should not infer from this that the discrepancies are due solely to nonsimilar effects. The integral method is, after all, an approximate method of solution and has some quantitative limitations.

In Fig. 7, the convective and radiative heat-transfer distributions on a hemisphere cone with a 30° half-angle are presented. There is a transition section between the hemisphere and the conical afterbody, as indicated in Fig. 7. The body curvature decreases continuously from unity to essentially zero in this region. The use of a transition section was found necessary to avoid large discontinuities in body curvature. The body shape is, for all practical purposes, a hemisphere cone. The reduction in both the convective and radiative heat transfer from the zero radiation loss value due to radiation cooling is seen to persist far downstream of the stagnation point. Note, however, that the convective heat transfer approaches its zero radiation loss value much more rapidly than is the case for radiative heat transfer. This is not surprising, since radiation is more sensitive to changes in enthalpy than is convection.

Also shown, for comparison purposes, is the convective heat-transfer distribution based on the pressure distribution obtained from the present results and the similar boundary-layer solution of Cohen.[18] The stagnation-point value was obtained from Ref. 20. The present results for the convective heat-transfer distribution with zero radiation loss are generally below the boundary-layer values, especially in the transition region. The relative trends exhibited by the solutions with and without radiation loss, however, are felt to be correct. A slight correction to the radiative heat-transfer distribution has been made to account for inaccuracies in the polynomial representation of the total enthalpy. The present solution was found to give total enthalpies slightly greater than the value behind the shock in some portions of the shock layer. The corrected radiative heat-transfer distribution was obtained by setting the total enthalpy equal to the value behind the shock whenever the solution indicated a larger value.

Velocity, total enthalpy, static enthalpy, and radiant emission profiles at several points on the body are shown in Figs. 8a–8d. Before we proceed to the discussion of Figs. 8a–8d, it should be noted that the radiative heating level for the equivalent pure cone is 3 Btu/ft^2 sec, which is about two orders of magnitude less than the present hemisphere-

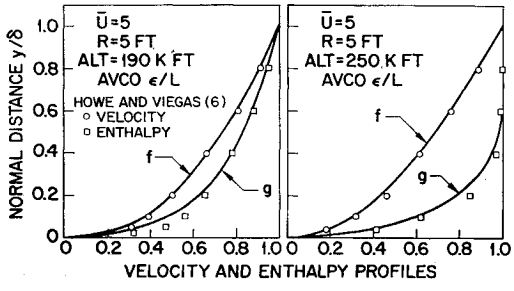

Fig. 5 Stagnation-point shock-layer profiles.

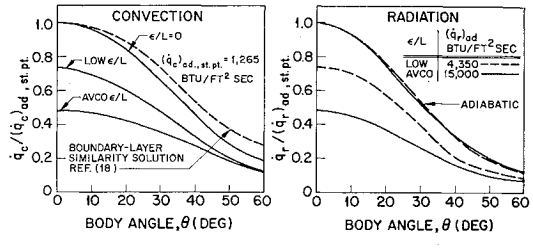

Fig. 6 Convective and radiative heat-transfer distribution on a hemisphere, $\bar{U} = 5$, alt = 190,000 ft, $R = 5$ ft.

cone value. This large difference in the radiative heating levels is due to the entropy layer. The important role of the entropy layer in determining the radiative heating level on the conical afterbody will be clearly demonstrated in the ensuing discussion of the velocity, enthalpy, and emission profiles.

Stagnation-point profiles are presented in Fig. 8a. The total enthalpy is seen to be decreased by radiation cooling, whereas the velocity profiles are quite similar for the cases with and without radiation loss. One must bear in mind, however, that, although the profiles are similar, the shock-detachment distance is decreased by radiation cooling so that the actual velocity field is altered. A radiation-cooled layer cannot be identified in Fig. 8a, since the viscous layer is sufficiently thick to swallow the radiation-cooled layer.

The emission profiles show that, at the stagnation point, the gas near the shock emits more than the gas near the wall. The quantity $\tilde{E}$ is proportional to the local emission and is used to calculate the radiative heat flux to the body surface by means of the following expression:

$$\frac{\dot{q}_R}{\rho_\infty U_\infty^3} = \frac{2\sigma\tilde{\lambda}_1\tilde{T}_1^4 R'}{\bar{\rho}_0 U_\infty^3}\,\tilde{\delta}\int_0^1 \tilde{E}\,d\eta$$

Downstream of the stagnation point, the emission attains a maximum within the shock layer, as shown in Figs. 8b–8d. As we proceed from the shock to the body, the emission increases since the static enthalpy increases. The increase in static enthalpy is caused by the decrease in velocity in the entropy layer, since the total enthalpy is essentially constant. Near the wall, the total enthalpy decreases due to heat transfer to the wall, and the static enthalpy and the emission both decrease. At a body location of $\xi = 1.52$ (Fig. 8c), the maximum emission in the shock layer is about 10^3 times as large as the emission immediately behind the shock. This demonstrates that the entropy layer is extremely important in determining the radiative flux on the conical afterbody in that it can increase the heating level by several orders of magnitude. At the body location $\xi = 2.93$, the entropy layer is beginning to thin out, and the emission remains at the value behind the shock some distance into the shock layer. The emission then increases to a value about 10^2 times as large as the value behind the shock. This behavior of the emission profile explains why the radiative heat transfer at $\xi = 2.93$ (Fig. 7) is so much higher than the pure cone value. These results indicate that sharp-nosed cones are more desirable since the entropy layer thins out as $\xi = x/R$ increases.

The effect of the entropy layer on the convective heat transfer is automatically taken into account since the shock layer is completely viscous. Its effect on convection is, however, a second-order effect.

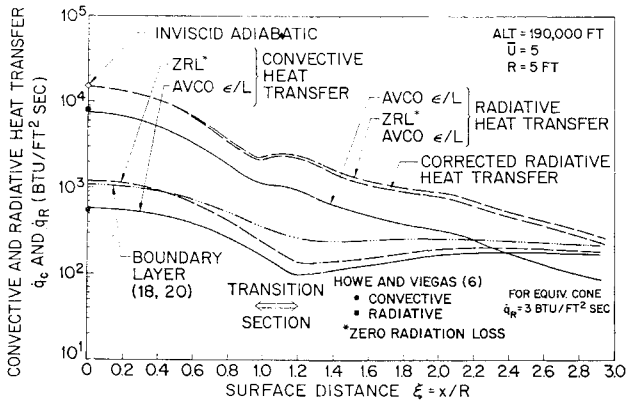

Fig. 7 Convective and radiative heat-transfer distribution on a hemisphere cone with 30° half-angle.

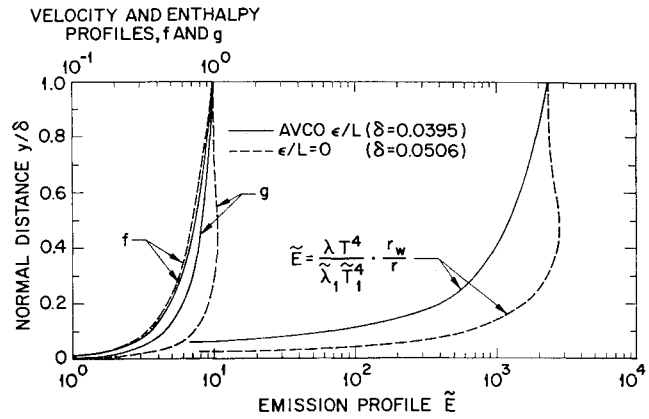

Fig. 8a Velocity, enthalpy, and emission profiles at $\theta = 0$, $\xi = 0$.

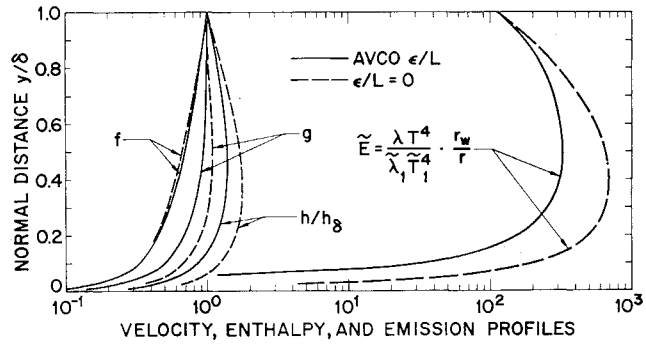

Fig. 8b Velocity, enthalpy, and emission profiles at $\theta = 50°$, $\xi = 0.873$.

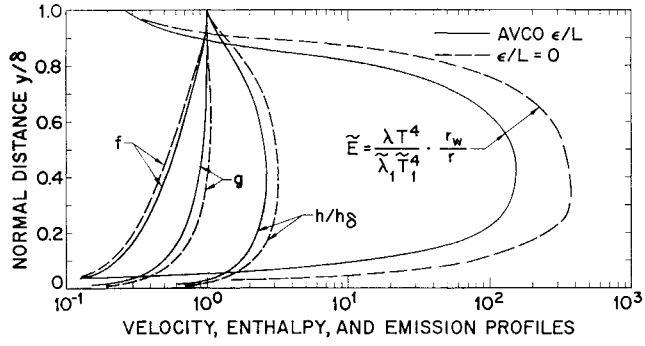

Fig. 8c Velocity, enthalpy, and emission profiles at $\theta = 60°$, $\xi = 1.52$.

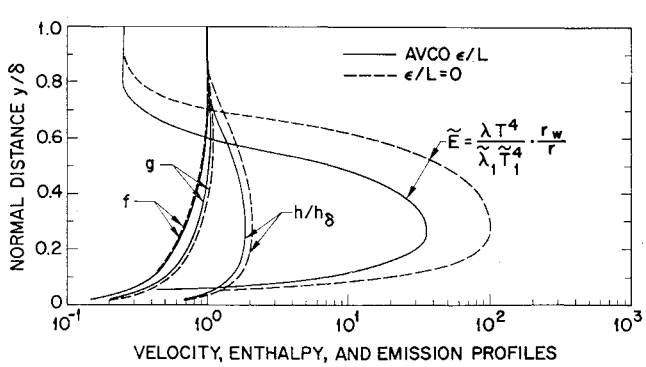

Fig. 8d Velocity, enthalpy, and emission profiles at $\theta = 60°$, $\xi = 2.93$.

6. Conclusions

The results of the present analysis show that the convective and radiative heat transfer are reduced by radiation-cooling losses. This reduction was found to persist around the body.

On the conical afterbody, the entropy layer can increase the radiative heating by orders of magnitude. This phenomenon indicates the desirability of pointed bodies to minimize the radiative heat transfer.

References

[1] Bird, G. A., "The effect of thermal radiation on the inviscid hypersonic flow over a blunt body," J. Aerospace Sci. **27**, 713–714 (1960).

[2] Wilson, K. H. and Hoshizaki, H., "Inviscid, nonadiabatic flow about blunt bodies," AIAA J. **3**, 67–74 (1965).

[3] Kennet, H., "Radiation-convection interaction around a sphere in hypersonic flow," ARS J. **32**, 1616–1618 (1962).

[4] Lighthill, M. J., "Dynamics of a dissociating gas. Part 1, Equilibrium flow," J. Fluid Mech. **2**, 1–32 (1957).

[5] Goulard, R., "The coupling of radiation and convection in detached shock layers," J. Quant. Specty. Radiative Transfer **1**, 249–257 (December 1961).

[6] Howe, J. T. and Viegas, J. R., "Solutions of the ionized radiating shock layer, including readsorption and foreign species effects and stagnation region heat transfer," NASA TRR-159 (1963).

[7] Thomas, P. D., "On the transparency assumption in hypersonic radiative gas dynamics," AIAA Preprint 64-434 (June 1964).

[8] Belotserkovskii, O. M., "On the calculation of flow past axisymmetric bodies with detached shock waves using an electronic computing machine," Prikl. Mat. Mech. **24**, 511–517 (1960).

[9] Van Dyke, M., "Higher approximations in boundary-layer theory," LMSC-703097, Lockheed Missiles & Space Co., Palo Alto, Calif. (October 1960).

[10] Maslen, S. H. and Moeckel, W. E., "Inviscid hypersonic flow past blunt bodies," J. Aerospace Sci. **24**, 683–693 (1957).

[11] Schlichting, N., "Boundary layer theory. Part 1, Laminar flows," NACA TM 1217 (April 1949).

[12] Scala, S. M., "The equations of motion in a multicomponent chemically reacting gas," Aerophysics Operation Research Memo. 5, General Electric Co., Missile and Ordnance Systems Dept., Philadelphia, Pa. (1957).

[13] Hirschfelder, J. O., "Heat transfer in chemically reacting mixtures. I," J. Chem. Phys. **26**, 274–285 (1957).

[14] Hansen, C. F., "Approximations for the thermodynamic and transport properties of high-temperature air," NASA TR R-50 (1959).

[15] Viegas, J. R. and Howe, J. T., "Thermodynamic and transport property correlation formulas for equilibrium air from 1,000°K to 15,000°K," NASA TN D-1429 (October 1962).

[16] Kivel, B. and Bailey, K., "Tables of radiation from high temperature air," Avco-Everett Research Lab., Research Rept. 21 (1957).

[17] Marrone, P. V., "Normal shock waves in air: Equilibrium composition and flow parameters for velocities from 26,000 to 50,000 fps," Cornell Aeronautical Lab. Rept. AG-1729-A-2 (August 1962).

[18] Cohen, N. B., "Boundary-layer similar solutions and correlation equations for laminar heat transfer distribution in equilibrium air at velocities up to 41,000 feet per second," NASA TR R-118 (1961).

[19] Libby, P. A., "The laminar hypersonic heat transfer on a blunt body according to the integral method," Heat Transfer Fluid Mech. Inst., 216–230 (June 1958).

[20] Hoshizaki, H., "Heat transfer in planetary atmospheres at super-satellite speeds," ARS J. **32**, 1544–1552 (1962).